Inorg. Chem. **2007**, *46*, 1771–1777

Computational Studies of Structures and Properties of Metallaboranes. Part 3: Protonated Iron Bis(dicarbollide), $[3\text{-Fe-}(1,2\text{-}C_2B_9H_{11})_2H]^-$

Michael Bühl,*,† Drahomír Hnyk,*,‡ and Jan Macháček‡

Institute of Inorganic Chemistry, Academy of Sciences of the Czech Republic, CZ-250 68 Řež near Prage, Czech Republic, and Max-Planck-Institut für Kohlenforschung, Kaiser-Wilhelm-Platz 1, D-45470 Mülheim an der Ruhr, Germany

Received November 3, 2006

On the basis of the energies and ^{11}B NMR chemical shifts computed at the BP86/AE1(*) and GIAO-B3LYP/II′ levels of density functional theory, respectively, the structure of the long-known protonated iron(II) bis(dicarbollide) can be assigned to a staggered isomer with a cisoid conformation of the carborane ligands. In the unprotonated species, in contrast, these ligands adopt the usual trans orientation, suggesting that suitable control of protonation/deprotonation equilibria could induce rotary motion at the molecular level.

1. Introduction

Protonated ferrocene is a textbook example[1] of electrophilic attack on a transition-metal complex. Ever since the determination of its sandwich structure, ferrocene has remained a landmark in organometallic chemistry,[2] and it continues to attract the interest of experimentalists and theoreticians alike. Recent computational studies, for example, have employed density-functional-based molecular dynamics simulations[3] and electron-correlated ab initio methods up to sophisticated coupled-cluster levels.[4] Computational characterization of the protonation product is complicated by its fluxionality and sensitivity to the particular methodology applied.[3]

Isolobal replacement of the cyclopentadienyl ligand in ferrocene with various *nido*-shaped heteroborane clusters with open pentagonal belts affords a large assortment of ferrocene-like metallaheteroboranes,[5] with dicarbollide complexes such as $[3\text{-Fe-}(1,2\text{-}C_2B_9H_{11})_2]^{2-}$ (**1**, Chart 1)[6] being archetypical examples.[1,7] Similarly to ferrocene, **1** can be protonated to yield a compound formulated as $[3\text{-Fe-}(1,2\text{-}C_2B_9H_{11})_2H]^-$ (**2**).[8] Both **1** and **2** have been identified by ^{11}B NMR spectroscopy; whereas the former was subsequently characterized by X-ray crystallography,[9] the precise structure of the latter is still unknown. Theoretical computations of ^{11}B chemical shifts, which have long been established as a structural tool for boranes and carboranes,[10,11] have

Chart 1

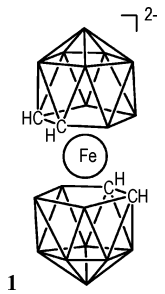

1

* To whom correspondence should be addressed. Fax: Int. code + (0)-208-3062996. E-mail: buehl@mpi-muelheim.mpg.de(M.B.),hnyk@iic.cas.cz (D.H.).

† Max-Planck-Institut für Kohlenforschung.

‡ Academy of Sciences of the Czech Republic.

(1) Elschenbroich, C. *Organometallics*, 3rd ed.; Wiley-VCH: Weinheim, Germany, 2006.

(2) See also a special issue on the 50th anniversary of the discovery of ferrocene: Adams, R. D. *J. Organomet. Chem.* **2001**, *637*, 1.

(3) Bühl, M.; Grigoleit, S. *Organometallics* **2005**, *24*, 1516.

(4) Coriani, S.; Haaland, A.; Helgaker, T.; Jorgensen, P. *ChemPhysChem* **2006**, *7*, 245.

(5) Štíbr, B. *J. Organomet. Chem.* **2005**, *690*, 2694.

(6) Hawthorne, M. F.; Young, D. C.; Andrews, T. D.; Howe, D. V.; Pilling, R. L.; Pitts, A. D.; Reintjes, M.; Warren, L. F., Jr.; Wegner, P. A. *J. Am. Chem. Soc.* **1968**, *90*, 879.

(7) For a review of iron bis(dicarbollides), see: Sivaev, I. B.; Bregadze, V. I. *J. Organomet. Chem.* **2000**, *614*, 27.

(8) Hawthorne, M. F.; Warren, L. F., Jr.; Callahan, K. P.; Travers, N. F. *J. Am. Chem. Soc.* **1971**, *93*, 2407.

(9) Kang, H. C.; Lee, S. S.; Knobler, C. B.; Hawthorne, M. F. *Inorg. Chem.* **1991**, *30*, 2024.

(10) (a) Bühl, M.; Schleyer, P. v. R. *J. Am. Chem. Soc.* **1992**, *114*, 477. (b) For a review, see: Bühl, M. In *Encyclopedia of Computational Chemistry*; Schleyer, P. v. R., Allinger, N. L., Kollman, P. A., Clark, T., Schaefer, H. F., Gasteiger, J., Schreiner, P. R., Eds.; Wiley: Chichester, U.K., 1998; p 1835.

(11) For a recent application of this structural tool [also called the ab initio-(DFT)/GIAO/NMR method] to boron compounds, see, e.g.: Bakardjiev, M.; Holub, J.; Štíbr, B.; Hnyk, D.; Wrackmeyer, B. *Inorg. Chem.* **2005**, *44*, 5826 and references therein.

10.1021/ic062096p CCC: $37.00
Published on Web 01/25/2007

recently been shown to hold great promise for metallacarboranes as well.[12,13] In fact, employing the modern tools of density functional theory (DFT), the molecular structure of **1** has been confirmed on the basis of a very good accord between computed and experimental $\delta(^{11}B)$ values for the transoid arrangement of the two dicarbollide moieties.[13] We now present a corresponding study for **2**, calling special attention to the location and possible fluxionality of the extra proton with respect to the metallacarborane moiety.

Further motivation for the present work was provided by the fact that some long-known transition-metal dicarbollides have recently found new potential applications in chemistry. For instance, the mutual rotation of the ligands in [3-Ni-(1,2-$C_2B_9H_{11})_2$] has been proposed as a basis for nanodevices.[14] The archetypical cobalt bis(dicarbollide), [3-Co-(1,2-$C_2B_9H_{11})_2]^-$, already used on an industrial scale in the reprocessing of nuclear waste,[15] has been found to act as a specific and potent inhibitor of HIV protease.[16] In the latter example, molecular recognition could be guided by dihydrogen H···H interactions between negatively polarized terminal hydrogens bound to boron and partially positive hydrogens in the amino acid residues.[17] Complexes of cobalt bis(dicarbollide) and its analogues with a simple Ala−Gly−Ala−Ala tetrapeptide, the latter modeling larger peptide chains, were investigated computationally to gain an alternative explanation for the inhibition mechanism.[18] In the latter study, both Co(III) and Fe(II) complexes proved to exhibit about the same interaction energy with the tetrapeptide. Because the affinity of the electron-rich metallacarborane toward acidic hydrogen atoms of the amino acids plays a decisive role in this process, we now focus on the interaction of **1** with a single proton, the ultimate electrophile. As it turns out, only a few stable minima can be located for the resulting protonation product, **2**, and the most stable of these have the dicarbollide ligands rotated from their relative positions in the reactant. It is thus conceivable that suitable control of the acid/base equilibrium between **1** and **2** could trigger rotary motion on the molecular level.

2. Computational and Experimental Details

Stationary points were optimized at the BP86/AE1(*) level, i.e., employing the exchange and correlation functionals of Becke[19] and Perdew,[20] respectively, together with a fine integration grid (75 radial shells with 302 angular points per shell) and a basis set consisting of the augmented Wachters' basis[21] on Fe (8s7p4d, full contraction scheme 62111111/3311111/3111) and the 6-31G* basis on all other elements (6-31G** for the extra proton).[22] This and comparable DFT levels have proven quite successful for transition-metal compounds and are well suited for the description of structures, energies, barriers, etc.[23] The nature of the stationary points was verified by computations of the harmonic frequencies at that level. Transition states were characterized by a single imaginary frequency, and visualization of the corresponding vibrational modes ensured that the desired minima were connected. Energies are reported at the BP86 level with and without zero-point corrections, computed both in vacuo and using a polarizable continuum model (PCM) on the basis of the integral equation formalism[24] (employing a cavity around all atoms using UFF radii). Natural population analyses and topological (Bader) analyses[25] of the BP86/AE1(*) total electron densities were performed using the NBO[26] routines in Gaussian 03 and the Morphy program,[27] respectively.

Magnetic shieldings were computed for all three BP86-geometry-optimized isomers and one transition state employing gauge-including atomic orbitals (GIAOs),[28] and the BP86 and hybrid B3LYP[29] functionals together with basis II′. The latter consists of the basis set on Fe as described above, a contracted (5s4p1d) Huzinaga basis of polarized triple-ζ quality on C and B, a double-ζ basis (2s) on H, and a polarized triple-ζ basis (3s1p) on the extra proton.[30,31] As for geometrical parameters, this particular combination of density functionals and basis sets has also turned out to perform well, particularly in terms of reproducing experimental $\delta(^{11}B)$ values, for this class of materials.[12,13]

^{13}C and ^{1}H chemical shifts are reported relative to TMS, computed at the same level (B3LYP C and H shielding constants of 181.1 and 31.7 ppm, respectively). ^{11}B chemical shifts were calculated relative to B_2H_6 (B3LYP B shielding constant of 81.4 ppm) and converted to the usual $BF_3{\cdot}OEt_2$ scale using the

(12) Bühl, M.; Hnyk, D.; Macháček, J. *Chem. Eur. J.* **2005**, *11*, 4109.
(13) Bühl, M.; Holub, J.; Hnyk, D.; Macháček, J. *Organometallics* **2006**, *25*, 2173.
(14) (a) Hawthorne, M. F.; Zink, J. I.; Skeleton, J. M.; Bayer, M. J.; Liu, Ch.; Livshits, E.; Baer, R.; Neuhauser, D. *Science* **2004**, *303*, 1849. (b) Hawthorne, M. F.; Ramachandran, B. M.; Kennedy, R. D.; Knobler, C. B. *Pure Appl. Chem.* **2006**, *78*, 1299. Review: (c) Kay, E. R.; Leigh, D. A.; Zerbetto, F. *Angew. Chem., Int. Ed.* **2007**, *46*, 72.
(15) See: Plešek, J. *Chem. Rev.* **1992**, *92*, 269 and references therein.
(16) Cígler, P.; Kožíšek, M.; Řezáčová, P.; Brynda, J.; Otwinowski, Z.; Pokorná, J.; Plešek, J.; Grüner, B.; Doleček ová-Marešová, L.; Máša, M.; Sedláček, J.; Bodem, J.; Kraeusslich, H. G.; Král, V.; Konvalinka, J. *Proc. Natl. Acad. Sci. U.S.A.* **2005**, *102* (43), 15394.
(17) The interaction of hydrogens of amino acids with [*closo*-1-$CB_{11}H_{12}]^-$ has been studied; see: Fanfrlík, J.; Lepšík, M.; Horinek, D.; Havlas, Z.; Hobza, P. *ChemPhysChem* **2006**, *7*, 1100.
(18) Fanfrlík, J.; Hnyk, D.; Lepšík, M.; Hobza, P., submitted for publication.
(19) Becke, A. D. *Phys. Rev. A* **1988**, *38*, 3098.
(20) (a) Perdew, J. P. *Phys. Rev. B* **1986**, *33*, 8822. (b) Perdew, J. P. *Phys. Rev. B* **1986**, *34*, 7406.
(21) (a) Wachters, A. J. H. *J. Chem. Phys*. **1970**, *52*, 1033. (b) Hay, P. J. *J. Chem. Phys.* **1977**, *66*, 4377.
(22) (a) Hehre, W. J.; Ditchfield, R.; Pople, J. A. *J. Chem. Phys.* **1972**, *56*, 2257. (b) Hariharan, P. C.; Pople, J. A. *Theor. Chim. Acta* **1973**, *28*, 213.
(23) See, for instance: (a) Koch, W.; Holthausen, M. C. *A Chemist's Guide to Density Functional Theory*; Wiley-VCH: Weinheim, Germany, 2000, and the extensive bibliography therein. It should be noted that hybrid functionals such as B3LYP need not be superior to pure, gradient-corrected functionals, as far as geometries of transition-metal complexes are concerned; see, for example: (b) Barden, C. J.; Rienstra-Kiracofe, J. C.; Schaefer, H. F. *J. Chem. Phys.* **2000**, *113*, 690. (c) Bühl, M.; Kabrede, H. *J. Chem. Theor. Comput.* **2006**, *2*, 1282.
(24) (a) Mennucci, B.; Tomasi, J. *J. Chem. Phys.* **1997**, *106*, 5151. (b) Mennucci, B.; Cancès, E.; Tomasi, J. *J. Phys. Chem. B* **1997**, *101*, 10506. (c) Tomasi, J.; Mennucci, B.; Cancès, E. *J. Mol. Struct. (THEOCHEM)* **1999**, *464*, 211. (d) Barone, V.; Cossi, M.; Tomasi, J. *J. Comput. Chem.* **1998**, *19*, 404. (e) Cossi, M.; Scalmani, G.; Rega, N.; Barone, V. *J. Chem. Phys.* **2002**, *117*, 43. (f) Cossi, M.; Crescenzi, O. *J. Chem. Phys.* **2003**, *19*, 8863.
(25) Bader, R. F. W. *Atoms in Molecules*; Oxford University Press: New York, 1990.
(26) Reed, A. E.; Curtiss, L. A.; Weinhold, F. *Chem. Rev.* **1988**, *88*, 899.
(27) Popelier, P. L. A. *Comput. Phys. Commun.* **1996**, *93*, 212.
(28) (a) Ditchfield, R. *Mol. Phys.* **1974**, *27*, 789. (b) Wolinski, K.; Hinton, J. F.; Pulay, P. *J. Am. Chem. Soc.* **1990**, *112*, 8251. (c) GIAO-DFT implementation: Cheeseman, J. R.; Trucks, G. W.; Keith, T. A.; Frisch, M. J. *J. Chem. Phys.* **1996**, *104*, 5497.
(29) (a) Becke, A. D. *J. Chem. Phys.* **1993**, *98*, 5648. (b) Lee, C.; Yang, W.; Parr, R. G. *Phys. Rev. B* **1988**, *37*, 785.
(30) Kutzelnigg, W.; Fleischer, U.; Schindler, M. In *NMR Basic Principles and Progress*; Springer-Verlag: Berlin, 1990; Vol. 23, pp 165−262.

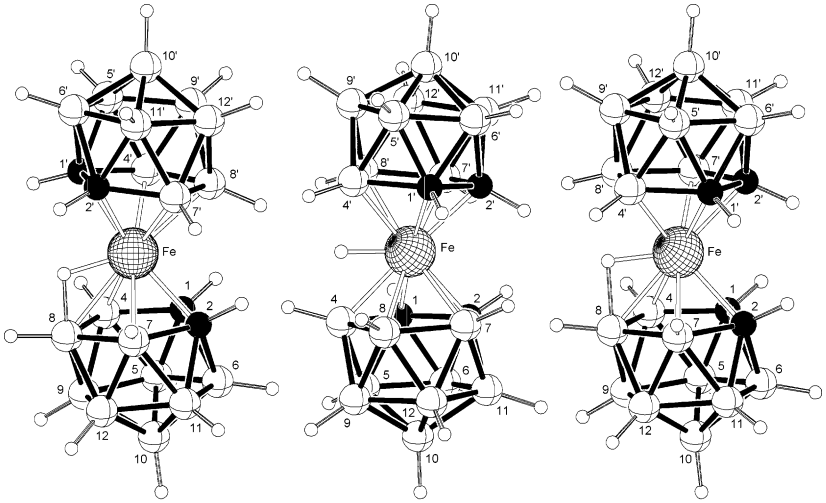

Figure 1. BP86/AE1(*)-optimized isomers of **2**, including labeling of nuclei.

experimental $\delta(^{11}B)$ value of B_2H_6, 16.6 ppm.[32] ^{57}Fe chemical shifts are reported relative to ferrocene, with a B3LYP shielding constant of −4503 ppm. All computations were performed with the Gaussian 03 program.[33]

3. Results and Discussion

3.1. Structures and Energies. Conformational analysis of **1** was reported in ref 13. Three minima with a staggered conformation of the two dicarbollide ligands that are rotamers along an axis passing through B10 and B10′ were located at the BP86/AE1 level (labeling analogous to that for **2** in Figure 1). The dihedral angle B8′−M−B10−B8 (θ) is a convenient measure for this rotation, assuming equilibrium values equal or close to 180° (**1a**), 108°, (**1b**), and 36° (**1c**). In accordance with experimental observation,[9] transoid **1a** is lowest in energy, being 4.6 and 19.1 kJ/mol more stable than **1b** and **1c**, respectively, at the BP86/AE1 level. Several protonation sites are conceivable for each of these minima. The extra proton could be metal-bonded, that is, located in the "equatorial plane" between the dicarbollide ligands and pointing in various radial directions, or it could be attached to any of the six B and four C atoms coordinated to the metal, potentially involved in agostic interactions with the latter, as is the case for protonated ferrocene.[3,34] A large number of corresponding starting structures was generated and optimized at the BP86/AE1(*) level (including a set of polarization functions on the extra proton, which has been found to be important for protonated ferrocene[3]). To ensure that no relevant minimum was missed, we also performed a two-dimensional relaxed potential energy surface scan, in which two fixed dihedral angles (H−Fe−B10−B8 and H−Fe−B10′−B8′) were scanned in increments of 36° (all other parameters optimized), followed by full optimization of the points of lowest energy. All of these many optimizations converged to one of just three minima, **2a**−**2c**, which adopt symmetries of C_s, C_2, and C_1, respectively (see plots in Figure 1). Selected internal coordinates and relative energies are listed in Tables 1 and 2, respectively.

Interestingly, only one protonated minimum can be found for each of the three rotamers of **1a**−**1c** (the parameters of the latter are included in Table 1 for comparison).[35] Symmetrical **2b** most closely resembles a metal-protonated form and has a short Fe−H distance of 1.496 Å, essentially identical to that in metal-protonated ferrocene at the same level (C_{2v} symmetry).[3] In **2a** and **2c**, interactions of the Fe-bonded H atom with one of the coordinated B atoms become apparent, with H···B distances as short as 1.336 Å in **2a** (Table 1), i.e., in a range typical for bridging BH bonds. There is precendence for a ferra-carborane with such a

(31) A reviewer has voiced concerns regarding the use of potentially unbalanced basis sets that do not contain polarization functions on all hydrogen atoms, but only on the "critical" proton. In our case, the presence or absence of such polarization functions on the terminal H atoms should have no significant effect on the relative energies and properties of the isomers. This expectation is borne out by some test calculations: For example, the relative energy of **2c** with respect to **2b** changes by no more than 0.2 kJ/mol upon going from the 6-31G(d) to the 6-31G(d,p) basis on the terminal H atoms. Similarly, the absolute ^{11}B shielding in B_2H_6 changes by less than 0.2 ppm upon going from basis II' to the full basis II with a (3s1p) basis on H. Effects on relative ^{11}B chemical shifts are expected to be even smaller. There is thus no evidence for any "unbalance" in the basis sets that we are using.

(32) Onak, T. P.; Landesman, H. L.; Williams, R. E.; Shapiro, I. *J. Phys. Chem.* **1959**, *63*, 1533.

(33) Frisch, M. J.; Trucks, G. W.; Schlegel, H. B.; Scuseria, G. E.; Robb, M. A.; Cheeseman, J. R.; Montgomery, J. A., Jr.; Vreven, T.; Kudin, K. N.; Burant, J. C.; Millam, J. M.; Iyengar, S. S.; Tomasi, J.; Barone, V.; Mennucci, B.; Cossi, M.; Scalmani, G.; Rega, N.; Petersson, G. A.; Nakatsuji, H.; Hada, M.; Ehara, M.; Toyota, K.; Fukuda, R.; Hasegawa, J.; Ishida, M.; Nakajima, T.; Honda, Y.; Kitao, O.; Nakai, H.; Klene, M.; Li, X.; Knox, J. E.; Hratchian, H. P.; Cross, J. B.; Adamo, C.; Jaramillo, J.; Gomperts, R.; Stratmann, R. E.; Yazyev, O.; Austin, A. J.; Cammi, R.; Pomelli, C.; Ochterski, J. W.; Ayala, P. Y.; Morokuma, K.; Voth, G. A.; Salvador, P.; Dannenberg, J. J.; Zakrzewski, V. G.; Dapprich, S.; Daniels, A. D.; Strain, M. C.; Farkas, O.; Malick, D. K.; Rabuck, A. D.; Raghavachari, K.; Foresman, J. B.; Ortiz, J. V.; Cui, Q.; Baboul, A. G.; Clifford, S.; Cioslowski, J.; Stefanov, B. B.; Liu, G.; Liashenko, A.; Piskorz, P.; Komaromi, I.; Martin, R. L.; Fox, D. J.; Keith, T.; Al-Laham, M. A.; Peng, C. Y.; Nanayakkara, A.; Challacombe, M.; Gill, P. M. W.; Johnson, B.; Chen, W.; Wong, M. W.; Gonzalez, C.; Pople, J. A. *Gaussian 03, revision B.01*; Gaussian, Inc.: Pittsburgh, PA, 2003.

(34) Karlsson, A.; Broo, A.; Ahlberg, P. *Can. J. Chem.* **1999**, *77*, 628.

(35) When optimizations of isomers of **2a**−**2c** with a different location of the proton in the equatorial belt were attempted, rearrangements (dicarbollide rotations) occurred during minimization, affording the original or another variant of **2a**−**2c**.

Table 1. Selected BP86/AE1(*)-Optimized Geometrical Parameters[a] for Isomers of **1** and **2**

isomer	θ[b]	M−C1/1′	M−C2/2′	M−B4/4′	M−B7/7′	M−B8/8′	C1/1′−C2/2′	C1/1′−B4/4′	C2/2′−B7/7′	B4/4′−B8/8′	B7/7′−B8/8′	φ[c]	α[d]	H−Fe	H−X1/2[e]
1a[f]	180.0	2.029	2.029	2.109	2.109	2.162	1.637	1.715	1.715	1.785	1.785	180.0			
expt[g]	180.0	2.015	2.047	2.073	2.112	2.144	1.616	1.671	1.720	1.808	1.792	180.0			
1b[f]	115.3	2.029	2.033	2.106	2.110	2.156	1.636	1.713	1.707	1.793	1.788	177.6			
1c[f]	43.8	2.030	2.033	2.107	2.108	2.156	1.639	1.713	1.712	1.794	1.792	175.9			
2a	180.0	2.058/2.066	2.058/2.066	2.165/2.147	2.165/2.147	2.227/2.189	1.634/1.660	1.686/1.690	1.686/1.690	1.864/1.789	1.864/1.789	169.5	0.0	1.540	1.336/2.232
2b	118.3	2.066	2.056	2.115	2.132	2.192	1.610	1.729	1.716	1.848	1.769	172.4	55.9	1.496	1.632/2.162
2c	46.2	2.062/2.069	2.062/2.063	2.142/2.133	2.138/2.136	2.149/2.173	1.638/1.628	1.689/1.696	1.670/1.704	1.853/1.842	1.835/1.788	171.5	4.0	1.509	1.468/1.953 (1.983)
TS2cc′	39.8	2.066	2.064	2.142	2.135	2.150	1.638	1.690	1.702	1.856	1.811	172.0	18.4	1.498	1.653

[a] Distances in angstroms, angles in degrees. [b] Dihedral angle B8′−Fe−B10−B8. [c] Angle B10−Fe−B10′. [d] Dihedral angle H−Fe−B10−B8. [e] X1/2 denote the closest/next-closest skeletal atoms, i.e., B8/C1′,2′ for **2a**, B4,4′/8,8′ for **2b**, B8/B4′(B8′) for **2c**, and B8 for **TS2cc′**. [f] From ref 13. [g] NMe_4^+ salt, ref 9.

Table 2. Relative Energies (kJ/mol) of Isomers of **2**

isomer	BP86/AE1(*)	BP86/AE1(*) + ZPE[a]	BP86/AE1(*) with PCM[b]	BP86/AE1(*) with PCM + ZPE[c]
2a	21.0	25.7	27.6 (28.5)	30.8 (31.5)
2b	0.0	0.0	7.7 (6.9)	6.5 (6.6)
2c	1.7	3.2	0.0	0.0
TS2ab	28.1	32.1	34.8	37.3
TS2bc	12.2	14.8	12.6	13.7
TS2cc	16.0	16.2	10.6	9.3
TS2cc′	2.5	1.1	−0.9 (0.2)	−3.8 (−2.7)

[a] Zero-point energies calculated at the BP86/AE1(*) level. [b] Polarized continuum model employing the parameters of water; single-point calculations on gas-phase geometries (in parentheses are PCM fully optimized energies). [c] PCM single points on gas-phase energies including gas-phase ZPEs (in parentheses are PCM-optimized energies with PCM-computed ZPE corrections).

bridging H atom, namely, in dinuclear $(Et_2C_2B_4H_4)Fe(H)(C_5Me_4{-}C_6H_4{-}C_5Me_4)Fe(H)(Et_2C_2B_4H_4)$,[36] where this H atom is involved in a four-center bond with two adjacent B atoms.[37]

Closer inspection of the BP86/AE1(*) wave function for **2c** reveals bonding interactions between the extra proton and B4/B4′ as well. These are apparent in the sizable Wiberg bond index (0.24 between that H and B4, essentially the same as for H−Fe, 0.23), as well as in the bond paths between these nuclei and the noticeable charge polarization visible in the Laplacian of the total electron density (Figure 2).

At the BP86/AE1(*) level, **2b** and **2c** are very close in energy (essentially isoenergetic; see Table 2)[38] and are significantly more stable than **2a** (by ca. 21 kJ/mol). Inclusion of zero-point corrections does not affect this qualitative picture (compare the BP86 and BP86 + ZPE entries in Table 2). The energetic ordering of the rotamers is thus completely different in **2** and **1**, where the transoid form **1a** is preferred.

In context with the ^{11}B NMR spectra discussed below, barriers for interconversion among the isomers **2a**−**2c** are

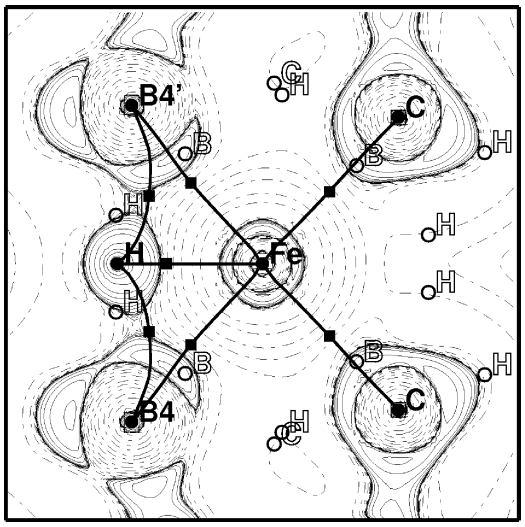

Figure 2. Topological analysis of the BP86/AE1(*) electron density in 2b: bond paths and Laplacian $-\nabla\rho$ in the plane containing the extra proton (bold H), Fe, B4, and B4′; contour lines are at $\pm 2^n \times 10^i$ au ($n = 1, 2, 3$; $i = 2, 1, ..., -3$). Note the bond paths between H and B4/B4′, as well as the "deformation" of the Laplacian around H toward the B atoms.

of interest, particularly those that scramble individual boron sites. Selected transition states for such processes were located, and the resulting (partial) energy profile is sketched in Figure 3. The two lowest minima, **2b** and **2c**, can interconvert via **TS2bc**, with a computed barrier of ca. 15 kJ/mol (including zero-point energy; Figure 3). A similar barrier, ca. 16 kJ/mol, was obtained for a degenerate rearrangement of **2c** via C_{2v}-symmetric **TS2cc**. It is noteworthy that this saddle point is even lower in energy than the minimum **2a**. For unprotonated **1**, in contrast, the corresponding C_{2v}-symmetric transition state (with $\theta = 0°$) is the highest point on the rotational profile (39.2 kJ/mol at BP86/AE1).[13]

A second degenerate rearrangement process in **2c** was investigated, namely, transfer of the extra proton from B8 to B8′ via C_2-symmetric **TS2cc′**.[39] On the potential energy surface, at the BP86/AE1(*) level, this transition state is only 0.8 kJ/mol above **2c**, in keeping with the fact that only minor geometric distortions are necessary to go from one stationary

(36) Stephan, M.; Davis, J. H., Jr.; Meng, X.; Chase, K. J.; Hauss, J.; Zenneck, U.; Pritzkow, H.; Siebert, W.; Grimes, R. N. *J. Am. Chem. Soc.* **1992**, *114*, 5214. This article also contains references to studies of other small metallcarboranes with this structural feature.

(37) Apparently, the nature of the Fe−H−B bridge, as three-center or four-center, can depend on the nature of the carborane ligand. The four-center bond found in ref 36 is qualitatively reproduced at the BP86/AE1(*) level for a pruned model, $Fe(C_5H_5)(C_2B_4H_6)H$ [optimized, Fe−H = 1.673 Å, mean = B−H 1.423 Å; observed for substituted derivative, Fe−H = 1.63(3) Å, B−H = 1.45(3) Å].

(38) The same was found at the B3LYP/II′ level, where **2c** is slightly more stable than **2b**, by 0.2 kJ/mol.

(39) The difference between **TS2cc** and **TS2cc′** is that the latter scrambles, among others, only B4 with B4′ and B7 with B7′, whereas the former scrambles all four of these.

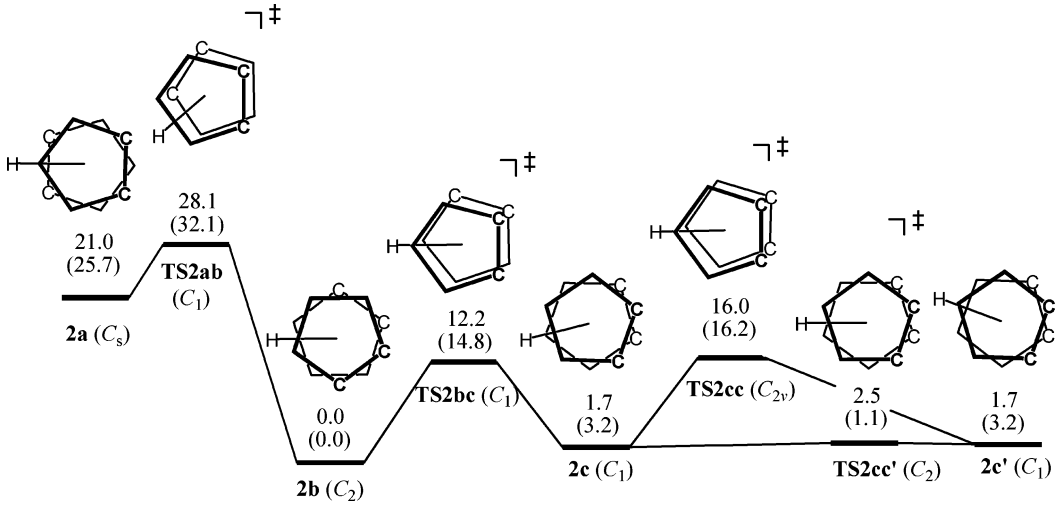

Figure 3. Schematic partial energy profile for rotation of the two dicarbollide ligands in **2**. Only the B_3C_2 pentagonal faces of these ligands are shown (boron atoms as vertices), and relative energies (in kJ/mol) are given at the BP86/AE1(*) level (in parentheses are the energies including zero-point corrections at the same level).

Table 3. GIAO-B3LYP/II′ Chemical Shifts[a] for **2a**−**2c** in Vacuo and in a Continuum

isomer	B(10,10′)	B(8,8′)	B(4,7,4′,7′)	B(9,12,9′,12′)	B(5,11,5′,11′)	B(6,6′)	C(1,2,1′,2′)	H	Fe
2a	−4.3 (−2.3, −6.3)	−12.9 (−29.3, 3.1)	−8.0 (−9.7, −9.7, −6.3, −6.3)	−12.8 (−14.7, −14.7, −10.9, −10.9)	−26.8 (−26.8, −26.8, −26.7, −26.7)	−22.7 (−20.1, −25.3)	58.8 (65.7, 65.7, 51.9, 51.9)	0.1	225
2b	−4.5 (−4.5, −4.5)	0.8 (0.8, 0.8)	−11.4 (−15.9, −6.9, −15.9, −6.9)	−12.1 (−13.0, −11.1, −13.0, −11.1)	−22.4 (−22.1, −27.7, −22.1, −22.7)	−29.6 (−29.6, −29.6)	57.9 (48.6, 67.3, 48.6, 67.3)	11.4	−522
2c	−5.1 (−4.2,−6.1)	−8.7 (−16.3, −1.1)	−9.8 (−10.4, −10.0, −11.7, −7.3)	−10.7 (−10.9, −11.6, −10.2, −10.0)	−25.6 (−25.9, −27.2, −25.1, −24.1)	−26.5 (−24.9, −28.1)	61.9 (66.0, 64.2, 58.2, 59.1)	9.8	−534
TS2cc′	−5.1 (−5.1,−5.1)	−8.4 (−8.4,−8.4)	−10.3 (−11.6, −11.6, −9.0, −9.08)	−10.3 (−10.0, −10.0, −10.6,−10.6)	−25.6 (−25.5, −25.5, −25.7, −25.7)	−26.6 (−26.6, −26.6)	62.7 (62.2, 62.2, 63.1, 63.1)	11.2	−725
2a (PCM)	−5.1 (−2.6, −7.7)	−14.2 (−29.3, 0.9)	−8.2 (−9.6, −9.6, −6.8, −6.8)	−14.0 (−15.3, −15.3, −12.7, −12.7)	−26.7 (−26.6, −26.6, −26.8, −26.7)	−21.9 (−19.4, −24.5)	59.6 (66.3, 66.3, 52.9, 53.0)	0.6	235
2b (PCM)	−5.3 (−5.3, −5.3)	−0.7 (−0.7, −0.7)	−11.6 (−16.2, −6.9, −16.2, −6.9)	−13.5 (−14.4, −12.7, −14.4, −12.7)	−22.2 (−22.2, −22.3, −22.2, −22.3)	−28.5 (−28.5, −28.5)	59.4 (50.0, 68.8, 50.0, 68.8)	11.3	−510
2c (PCM)	−5.7 (−4.4, −6.9)	−10.2 (−17.0, −3.4)	−10.3 (−11.2, −9.9, −12.2, −8.0)	−12.3 (−12.2, −12.9, −12.0, −12.0)	−25.2 (−25.7, −26.2, 25.2, 23.7)	−25.0 (−23.4, −26.6)	63.2 (67.0, 65.3, 60.3, 60.4)	9.5	−554
expt[b]	*−2.5*	*−8.9*	*−11.2*	*−12.5*	*−22.3*	*−22.3*			

[a] BP86/AE1(*) geometries, $\delta(^{11}B)$, $\delta(^{13}C)$, $\delta(^{1}H)$, and $\delta(^{57}Fe)$ relative to $BF_3{\cdot}OEt_2$, TMS, TMS, and ferrocene, respectively; dynamically averaged values are given (in parentheses: individual values in the static minima). [b] $Cs[Fe(C_2B_9H_{11})_2H]$ (20% $HClO_4/CH_3OH$), ref 40.

point to the other (cf. the geometrical parameters in Table 1). Inclusion of zero-point corrections brings the energy of **TS2cc′** even slightly below that of **2c**, suggesting that the former saddle point might be a better representation for the actual ground state than the latter minimum. It is to be expected that this finely balanced energy difference between **2c** and **TS2cc′** could be quite sensitive to the level of theory (similar to the situation for protonated ferrocene[3]). We did not explore this possibility further and just note that the potential energy surface is indicated to be quite flat around **2c**.

To summarize this section, **2** emerges from our DFT computations as a quite fluxional system with low barriers for rotation of the two dicarbollide ligands relative to each other. Most significantly, the relative orientation of these ligands is different in the lowest minima of **2** and **1**, suggesting that protonation/deprotonation equilibria between the two species could trigger fast rotary motion of these ligands. A similar situation was previously found for [3-Ni-(1,2-$C_2B_9H_{11}$)$_2$] and its radical cation: Because the two species have different equilibrium conformations, the redox process interconverting them has been proposed as a means to control this rotation and turn the complex into a very small molecular rotor.[14] Our results indicate that similar control might be achievable for **1**, for instance by tuning the pH value.

3.2. NMR Chemical Shifts. Calculated chemical shifts are collected in Table 3, together with the experimental values. The observed ^{1}H-coupled ^{11}B NMR spectrum was found to be difficult to interpret because of broad and overlapping lines.[8] We used the δ values extracted by Todd and Siedle from this spectrum[40] as reference values. In the

(40) Todd, L. J.; Siedle, A. R. *Prog. Nucl. Magn. Reson. Spectrosc.* **1979**, *13*, 87.

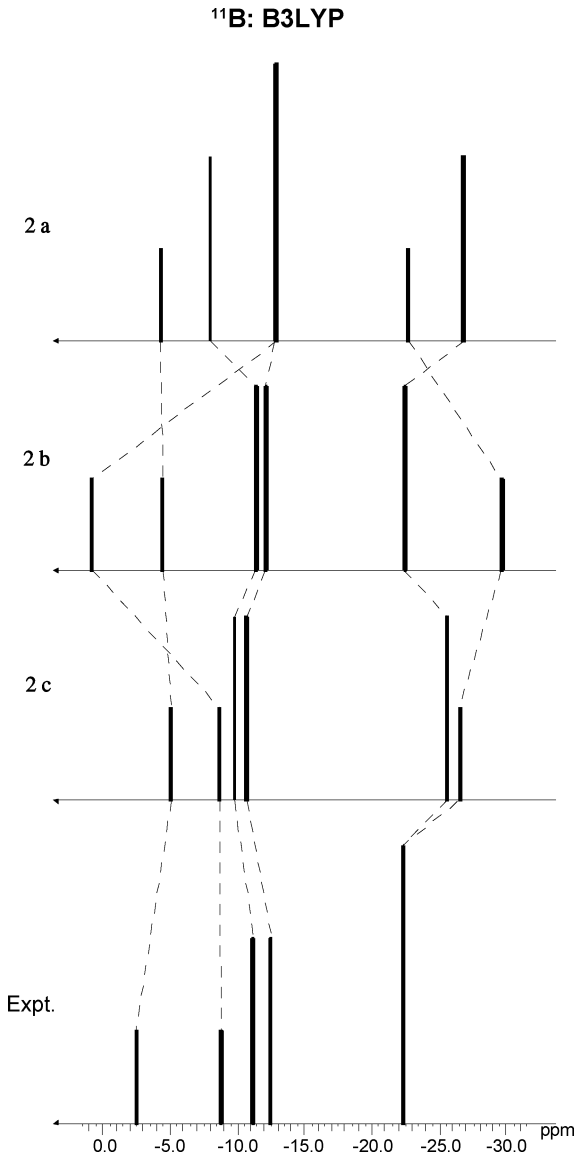

Figure 4. Schematic representations of experimental (bottom) and theoretical ^{11}B NMR spectra for 2, computed at the B3LYP/II′//BP86 level.

absence of definite assignments, we can only compare theoretical and experimental numbers on the basis of the best fit (taking the relative intensities into account).

The experimental ^{11}B NMR spectrum consists of five lines (one of which encompasses two sites, arguably because of accidental degeneracy), indicative of high apparent symmetry on the NMR time scale (C_{2h} or C_{2v}). As discussed in the preceding section, the rotational barriers connecting **2a**−**2c** are low enough for scrambling of the corresponding ^{11}B sites that are nonequivalent in the minima with lower symmetry. The highest point on the potential energy surface in Figure 3 that is necessary to scramble the ^{11}B chemical shifts in **2b** and **2c** to the observed symmetry is **TS2cc** (C_{2v}), which is only 16 kJ/mol above the lowest minimum. Thus, the minima are expected to be highly fluxional on the NMR time scale, and static spectra of the former could be "frozen out" only at very low temperatures. We therefore discuss only the correspondingly averaged calculated $\delta(^{11}\text{B})$ values (the individual static values are given in parentheses in Table 3).

Of the three minima, **2a** and **2c** show the best agreement with experiment; the two isomers have rather similar maximum deviations (**2a**, 4.5 ppm for B5 and B11; **2c**, 4.2 ppm for B6), as well as very similar mean absolute errors over all six resonances, i.e., 2.4 and 2.3 ppm for **2a** and **2c**, respectively. Isomer **2b** shows the worst fit, with mean absolute and maximum deviations of 2.6 and 7.3 ppm, respectively. The latter error (for B6) occurs for one of the two high-field resonances that are overlapping in the experiment. For **2b**, these two signals were computed to differ by more than 7 ppm, which is close to the error margin established in our previous validation studies (ca. 7 ppm at most), but which is clearly not compatible with the observed pattern. This mismatch is clearly apparent in the stick representations of the ^{11}B NMR spectra in Figure 4 (compare the two rightmost signals for **2b** with the experimental one).

To our knowledge, no other NMR parameters are known for **2**. The ^{1}H NMR signal of the extra proton was not observed, presumably because of exchange with solvent and/or line broadening due to traces of Fe(III).[8] As in the case of protonated ferrocene,[3,34] a symmetrical location of this proton between the two sandwich ligands (e.g., in **TS2cc′** or in **2b**) is associated with a strongly deshielded ^{1}H resonance, whereas a noticeable upfield shift is predicted in the case of a pronounced interaction with one B atom (e.g., in **2a**, see Table 3). Because the extra proton does not interact directly with a carbon atom in any of the compounds **2a**−**2c**, little discrimination is apparent between the computed ^{13}C chemical shifts in this set. As expected, the ^{57}Fe nucleus is more sensitive, with variations in $\delta(^{57}\text{Fe})$ approaching 1000 ppm. The low receptivity of this nucleus, however, will make the experimental test of our predicted values very difficult.[41]

By necessity, the experimental ^{11}B NMR spectrum was recorded under strongly acidic conditions, in a protic solvent with high polarity ($HClO_4$/MeOH). To assess the bulk-medium effect of such a polar environment on energies and chemical shifts, we finally evaluated the latter properties in the presence of a polarizable continuum (PCM). Lacking the dielectric constant of the actual solution, we employed the corresponding parameters of water in these PCM computations. The largest change of the computed ^{11}B chemical shifts on going from the gas phase to the continuum amounts to 1.7 ppm, and most values are affected by less than 1 ppm (Table 3). These are relatively minor modifications that do not alter the overall qualitative result, namely, that best accord with experiment is found for **2a** and **2c**, and a large discrepancy is apparent for **2b**.

Interestingly, on going from the gas phase to the continuum, the energetic sequence of the two lowest minima, **2b** and **2c**, is switched. Whereas the former is slightly more stable in the gas phase, it is the latter that is indicated to be somewhat more favored in a polar solvent (by 7 kJ/mol, cf.

(41) For protonated ferrocene, an ^{57}Fe chemical shift has been reported; see: (a) Koridze, A. A.; Petrovskii, P. V.; Gubin, S. P.; Fedin, E. I. *J. Organomet. Chem.* **1975**, *93*, C26. (b) Koridze, A. A.; Stakhova, N. M.; Petrovskii, P. V. *J. Organomet. Chem.* **1983**, *254*, 345.

PCM data in Table 2).[42,43] The transoid form **2a** was computed to be very high in energy throughout (on the order of 30 kJ/mol with PCM), suggesting that it can be excluded on energetic grounds.[44]

In view of the very small energetic difference between **2c** and **TS2cc′** (Figure 3), we also computed the chemical shifts for the latter transition state (last entry in Table 3). Even though some larger differences were found between individual boron sites in **2c** and **TS2cc′** (compare corresponding values in parentheses in Table 3), the dynamically averaged $\delta(^{11}B)$ values are very similar for the two structures (within ca. 3 ppm) and are both compatible with experiment. The precise location of the proton in the Fe−B8−B8′ plane of this isomer can thus not be determined at present, inviting further experimental and theoretical scrutiny.

4. Conclusions

According to DFT computations at the BP86/AE1(*) level, protonation of iron(II) bis(dicarbollide) can produce one of three distinct minima **2a**−**2c**, which differ in the mutual orientation of the staggered dicarbollide ligands. Assignment of the experimentally known species to one of these structures is effected by a combination of energetic and NMR criteria: One isomer, **2a** with a transoid arrangement of the two dicarbollide ligands, can be excluded because it is quite high in energy, ca. 25−30 kJ/mol above the two other minima. Discrimination of these two isomers, which are almost isoenergetic at the DFT level employed, can be achieved by the computed ^{11}B chemical shifts: It is only for cisoid C_1-symmetric **2c** (or a closely related transition state with C_2 symmetry) that the computed $\delta(^{11}B)$ values are in satisfactory agreement with the experimental NMR data from the literature. This isomer is thus indicated to be the one that was observed. Because it has a different conformation of the dicarbollide ligands compared to the unprotonated reactant and because the activation barriers for interconversion of individual isomers are computed to be quite low, iron(II) bis(dicarbollide) might be a potential candidate for a nanodevice delivering rotary motion upon protonation.

Acknowledgment. This work was supported by the German Academic Exchange Service (DAAD) and the Academy of Sciences of the Czech Republic in the joint PPP programme, as well as the Ministry of Education of the Czech Republic (Project LC 523). We thank Josef Holub for his interest in experimental aspects of this work. M.B. thanks Prof. W. Thiel and the MPI in Mülheim, Germany, for continuous support. Computations were performed on a local computer cluster of Compaq XP1000, ES40, and Intel Xeon workstations and PCs at the MPI Mülheim, Germany, maintained by Horst Lenk.

Supporting Information Available: Optimized geometries of all minima and transition states of **2** (Cartesian coordinates in *x*, *y*, *z* format). This material is available free of charge via the Internet at http://pubs.acs.org.

IC062096P

(42) An important reason for the stabilization of **2c** over **2b** in a polar environment is certainly the larger dipole moment of the former compared to that of the latter [4.8 D vs 2.6 D, respectively, at the BP86/AE1(*) level in vacuo; these values increase by ca. 70% each in solution]. Non-electrostatic contributions to the total free energy in solution (which are not included in the energies we report) are very similar for all isomers considered. It should be kept in mind that PCM approaches are very crude models that can, at best, describe long-range electrostatic interactions qualitatively, without accounting for specific solute−solvent interactions such as hydrogen bonds. We just note that the qualitative ordering of **2b** and **2c** as it emerges from the PCM data appears to be consistent with the results from the NMR computations.

(43) It should be noted that the energetic difference between these isomers is also very small in the continuum, arguably within the accuracy of our computational level. In this case, discrimination via the chemical shifts is more reliable.

(44) A good accord between computed and experimental chemical shifts cannot prove the correctness of the structure used in the computations, because the possibility cannot be excluded that two or more structures can show the same or very similar δ values. In that case, other criteria can be used to make a distinction, e.g., as in our case, relative energies. In contrast, a structure can be disproved in the case of a poor accord between theory and experiment, i.e., if it produces errors exceeding the usual accuracy of the computational method applied, as for **2b** in our case.